Palaeogeography, Palaeoclimatology, Palaeoecology 466 (2017) 153–165

Contents lists available at ScienceDirect

Palaeogeography, Palaeoclimatology, Palaeoecology

journal homepage: www.elsevier.com/locate/palaeo

Shallow-water carbonate responses to the Paleocene–Eocene thermal maximum in the Tethyan Himalaya (southern Tibet): Tectonic and climatic implications

Juan Li [a], Xiumian Hu [a,*], Eduardo Garzanti [b], Marcelle BouDagher-Fadel [c]

[a] State Key Laboratory of Mineral Deposit Research, School of Earth Sciences and Engineering, Nanjing University, Nanjing 210023, China
[b] Laboratory for Provenance Studies, Department of Earth and Environmental Sciences, Università di Milano-Bicocca, 20126 Milano, Italy
[c] Department of Earth Sciences, University College London, London WC1H 0BT, UK

ARTICLE INFO

Article history:
Received 11 June 2016
Received in revised form 31 October 2016
Accepted 16 November 2016
Available online 17 November 2016

Keywords:
PETM
Tethys Ocean
Carbonate platform
Disconformity
India-Asia collision
Carbon isotope excursion

ABSTRACT

This study presents a detailed stratigraphic record of the Paleocene–Eocene Thermal Maximum (PETM) in the Gamba area of the Tethyan Himalaya, a carbonate-platform succession originally deposited along the southern margin of the eastern Tethys Ocean. The Paleocene-Eocene boundary interval is marked by a negative carbon isotope excursion at the boundary between members 3 and 4 of the Zongpu Formation. The succession is erosionally truncated at this surface, which is overlain by an intraformational carbonate conglomerate, and only the upper part of the PETM interval is preserved. Foraminiferal assemblages of Shallow Benthic Zone 4 are present below the conglomerate bed, but are replaced by assemblages of Shallow Benthic Zone 6 above the conglomerate. Depositional facies also change across this surface; below the disconformity, floatstones and packstones containing nummulitid forams record progressive transgression in an open-marine environment, whereas restricted or lagoonal inner-ramp deposits containing *Alveolina* and *Orbitolites* are typical above the disconformity. The prominent negative excursion observed in the $\delta^{13}C$ of whole-rock carbonate (−1.0‰ at Zongpu, −2.4‰ at Zengbudong) and organic matter (−24.7‰, at Zengbudong) is correlated to the characteristic PETM carbon isotope excursion. This major negative excursion in shallow-marine carbonates may have partly resulted from syndepositional alteration of organic matter. The erosional unconformity can be constrained to the lower PETM interval (between 56 and 55.5 Ma), and is identifiable throughout the Tethyan Himalaya. This widespread disconformity is attributable to tectonic uplift associated with the southward migration of an orogenic wave, originated 3 ± 1 Ma earlier in the middle Paleocene at the first site of India-Asia continent-continent collision. A possible eustatic component of the pre-PETM sea-level fall, which resulted in the excavation of incised valleys filled during the subsequent sea-level rise when the conglomerate bed was deposited, remains to be assessed.

1. Introduction

The Paleocene–Eocene Thermal Maximum (PETM) was a geologically brief (~170–200 kyr) episode of globally elevated temperatures (Röhl et al., 2007; Murphy et al., 2010), superimposed on a longer-term late Paleocene to early Eocene warming trend, which culminated in the highest ocean temperatures of the Cenozoic (the early Eocene climatic optimum; Kennett and Stott, 1991; Zachos et al., 2001). The PETM was characterized by global warming of both the earth's surface and the deep oceans, by 5–8 °C (McInerney and Wing, 2011). Its onset is defined by a negative carbon isotope excursion (CIE) recorded worldwide (Dupuis et al., 2003). Although the ultimate cause and trigger of the CIE is uncertain (Sluijs et al., 2006), the dissociation of methane hydrates along continental margins is a plausible hypothesis that may explain the injection of large amounts of ^{13}C–depleted carbon into oceanic and atmospheric reservoirs (Dickens et al., 1997). Major global biotic changes occurred simultaneously with the CIE, including a major extinction of deep-sea benthic foraminifera, blooms of tropical and subtropical planktonic foraminifera, a turnover in 'larger benthic foraminifera', an increased abundance of dinoflagellates, and the disappearance of coral reefs (Bowen et al., 2006; Sluijs et al., 2007; Speijer et al., 2012). The onset of the CIE is an excellent global chemostratigraphic correlation tool (McInerney and Wing, 2011), and is formally used to define the base of the Eocene (Aubry et al., 2007).

To fully understand biotic responses to climate change during the PETM, detailed analyses of faunal and floral evolution are needed from a wide spectrum of different environments, including the deep oceans, shallow seas, and terrestrial settings. Despite major advances in our understanding of the PETM in open-marine environments, shallow-marine settings remain poorly explored, and the effects of this global climatic event on the widespread epeiric carbonate platforms of the

* Corresponding author.
E-mail address: huxm@nju.edu.cn (X. Hu).

http://dx.doi.org/10.1016/j.palaeo.2016.11.026
0031-0182/

Paleogene remain unclear. The Tethys Ocean was a vast, east-west trending subtropical seaway during the Paleogene, with neritic deposition occurring in a variety of environments along its margins, making it an excellent place to study the PETM in shallow-marine settings.

The thick shallow-marine carbonate succession of the Tethyan Himalaya spans the critical late Paleocene-early Eocene interval, and is characterized by abundant index fossils (Willems and Zhang, 1993; Hu et al., 2012; Zhang et al., 2013; Li et al., 2015), offering a rare opportunity to study a detailed, biostratigraphically controlled record of the PETM in the eastern Tethys. Biostratigraphy based on larger benthic foraminifera, coupled with precise carbon isotope chemostratigraphy, allows us to place firm constraints on the stratigraphic and environmental evolution of the Indian margin during the very first stages of the India-Asia collision, a period that spans the critical interval of the PETM.

2. Geologic setting and lithostratigraphy

The Tethyan Himalaya, situated between the Greater Himalaya to the south and the Indus-Yarlung-Zangbo Suture and Lhasa Block to the north (Fig. 1A), consists of sedimentary rocks originally deposited along the northern margin of the Indian continent. The Tethyan Himalaya is traditionally subdivided into southern and northern zones, separated by the Gyirong-Kangmar Thrust. The southern zone includes a Paleozoic to Eocene succession, composed largely of shelf carbonates and terrigenous deposits (Willems et al., 1996; Sciunnach and Garzanti, 2012), whereas the northern zone is dominated by deeper-water Mesozoic to Paleocene slope and rise sediments. Paleomagnetic data indicate that the Tethyan Himalaya was located at peri-equatorial latitudes in the latest Mesozoic and early Cenozoic, ranging from 5.6 ± 2.8° S during Campanian-Maastrichtian time to 10.1 ± 2.0° N during Selandian-Thanetian time (Yi et al., 2011).

Our study area is located in the southern Tethyan Himalaya, near the town of Gamba (Fig. 1B). The site has a continuously exposed marine sedimentary succession ranging from the Upper Cretaceous to Eocene, subdivided into three lithostratigraphic units (the Jidula, Zongpu and Enba formations). Lower Paleocene shoreface deposits of the Jidula Formation consist of quartzose sandstones derived from the Indian continent (Garzanti and Hu, 2015). The overlying Zongpu Formation is composed of thin- to massively-bedded fossiliferous limestones at the base, with nodular limestones in the middle and thick-bedded fossiliferous limestones in the upper part of the formation (Willems et al., 1996; Li et al., 2015). In the Gamba area, the Zongpu Formation can be further

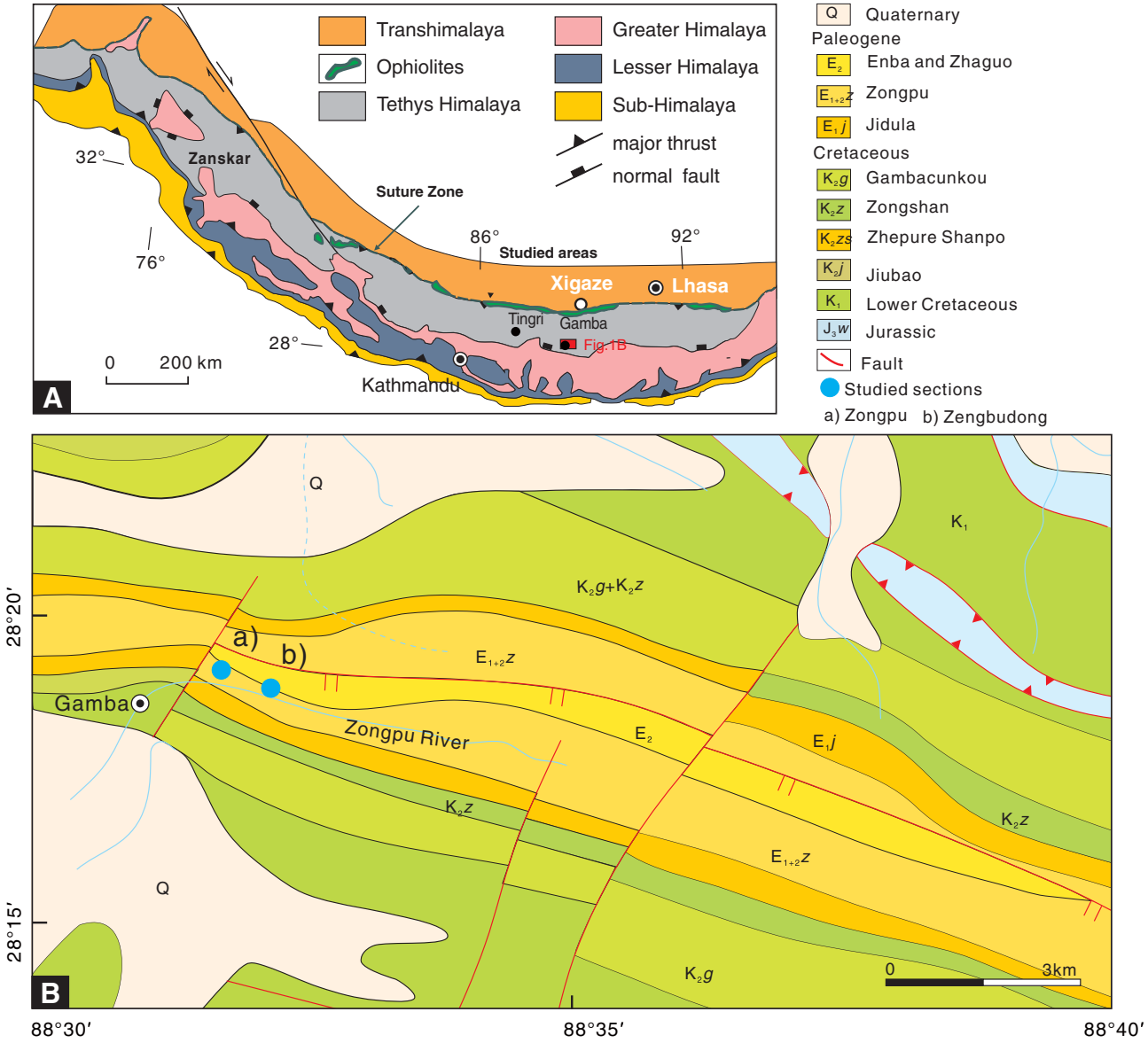

Fig. 1. A) Schematic geologic map of the Himalayan Range; B) Geologic maps of the Gamba area, showing the location of the studied sections.

subdivided into four members; thin- to medium-bedded limestones in member l, nodular limestones in member 2, nodular marly limestones in member 3, and thick- to massively-bedded limestones in member 4. Members 3 and 4 are separated by a lenticular conglomerate bed, marking an erosional disconformity that roughly corresponds to the Paleocene-Eocene boundary (Wang et al., 2010; Wan et al., 2002; Li et al., 2015; Fig. 2B, C, D). The Enba Formation comprises greenish-grey marls, intercalated in the upper part of the formation with litho-quartzose sandstones sourced from the Asian continent, and deposited in prodelta to offshore environments (Wan et al., 2002; Hu et al., 2012).

3. Materials and methods

3.1. Stratigraphic sections

We focused our study on the Zongpu Formation, by measuring two main sections in the Gamba area (Zongpu and Zengbudong), and sampling them in detail for petrographic, biostratigraphic and carbon isotope analysis (Fig. 1).

Microfacies analysis was carried out on 550 thin sections from the Zongpu section and 80 thin sections from the Zengbudong section using transmitted-light microscopy. This allowed us to make semiquantitative estimates of the main sedimentary components, as well as observe primary textural and diagenetic features, identify microfossils (with a special emphasis on larger benthic foraminifera), and interpret of depositional settings. Samples for isotope measurements were collected with an average spacing of 1 m, reduced to ~0.4 m across the Paleocene-Eocene boundary. Biostratigraphic correlations were based on the distribution of larger benthic foraminifera (identification based on Hottinger, 1960; BouDagher-Fadel, 2008). We used the Tethyan Shallow Benthic Zonation established by BouDagher-Fadel (2008, 2015). These shallow benthic biozones can be correlated with the well-established ranges of planktonic foraminifera (BouDagher-Fadel, 2013), in order to assign biostratigraphic ages to different intervals.

3.2. Carbon and oxygen isotopes

To assemble a detailed chemostratigraphic record of the studied sections, we analyzed whole-rock carbonate isotope values throughout the entire succession. We processed a total of 357 samples from the Zongpu section and 84 from the Zengbudong section. Powdered samples were obtained by micro-drilling, taking care to avoid cement-filled veins and pores, or larger bioclasts. The carbon and oxygen isotope ratios of powdered samples were measured at the State Key Laboratory for Mineral Deposits Research at Nanjing University, using a Finnigan MAT Delta Plus XP mass spectrometer coupled to an in-line GasBench II autosampler. Samples were reacted with purified orthophosphoric acid at 70 °C. Data are expressed in standard delta notation, as permil deviations from the Vienna Pee Dee Belemnite (VPDB) standard. Duplicate measurements of standards yielded an analytical precision (1σ) of 0.05‰ for $\delta^{13}C$ and 0.07‰ for $\delta^{18}O$.

To supplement our carbonate isotope results, we analyzed organic carbon isotopes across the critical Paleocene-Eocene boundary interval in the Zengbudong section. Thirty-eight samples were decarbonated using 10% HCl, and analyzed at the SINOPEC Wuxi Research Institute of Petroleum Geology, using a Finnigan MAT Delta Plus XL mass spectrometer. The results were corrected to the VPDB scale and are expressed using delta notation. Additionally, 14 limestone clasts collected from the conglomerate bed in the Zengbudong section were analyzed for both whole-rock carbonate and organic carbon isotopes.

4. Results

4.1. Lithostratigraphy

The sedimentology and stratigraphy of the Zongpu and Zengbudong sections are described in detail in Li et al. (2015). Here we focus on the stratigraphic interval immediately surrounding the Paleocene-Eocene boundary, and on the sedimentological features of the Paleocene-Eocene disconformity (Fig. 3).

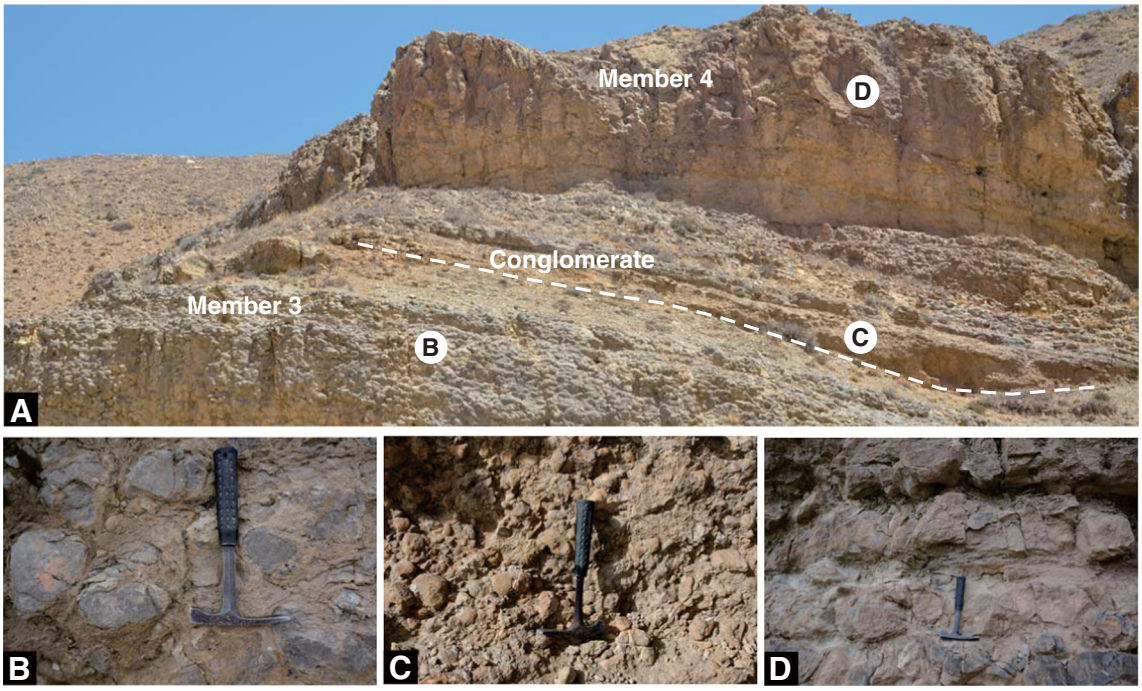

Fig. 2. Field photographs: (A) Member 3, conglomerate bed, and member 4 of the Zongpu Formation in the Zengbudong section, Gamba area; (B) nodular marly limestones of uppermost member 3; (C) the conglomerate bed in the Zongpu Formation, Gamba area; (D) thick- and massively-bedded limestones of member 4.

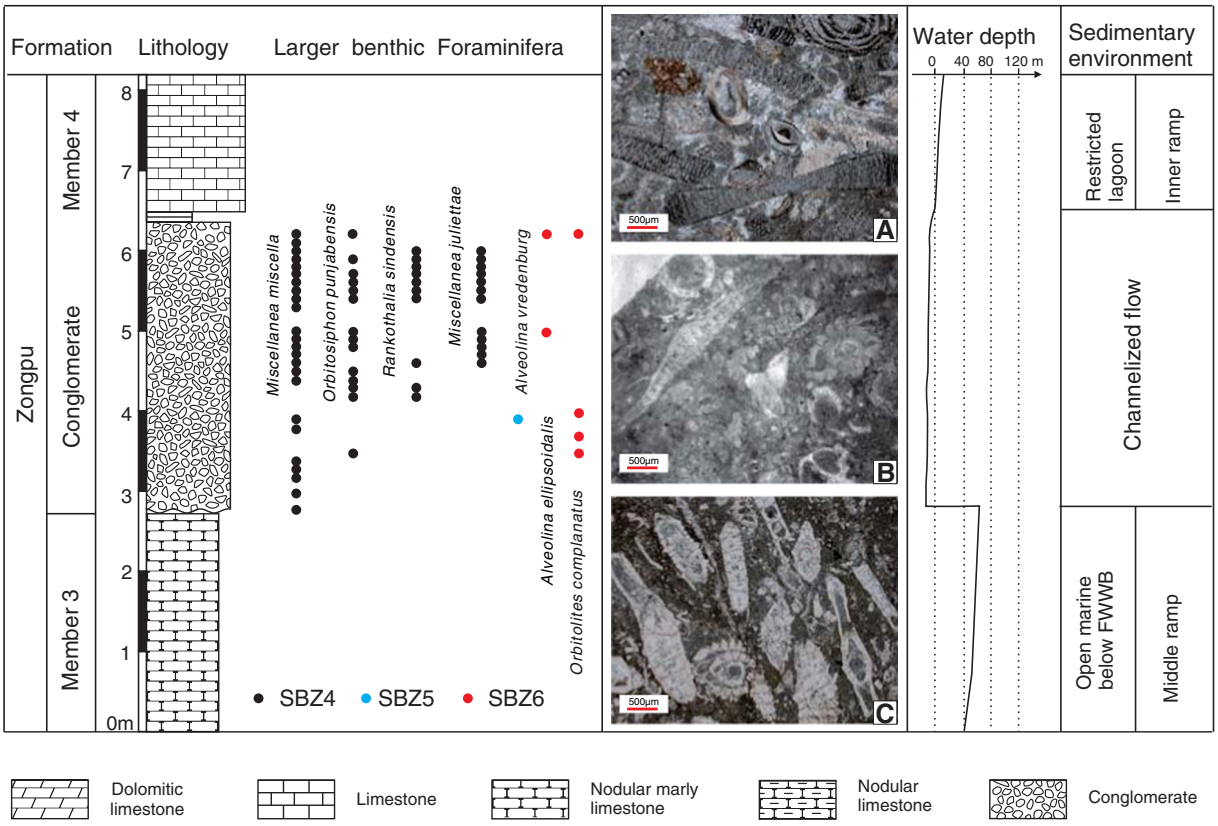

Fig. 3. Lithological log of the Zongpu Formation (Zongpu and Zengbudong sections) spanning the Paleocene/Eocene boundary, showing the distribution of larger benthic foraminifera, carbonate microfacies, interpreted palaeowater depths and depositional environments, and the distribution of larger benthic foraminifera in carbonate clasts of the conglomerate bed. A) Floatstone with *Alveolina* and *Orbitolites* in lowermost member 4; B) packstone with nummulitids in the carbonate clasts, from the conglomerate bed; C) packstone with nummulitids in uppermost member 3. SBZ = Shallow Benthic Zonation of Serra-Kiel et al. (1998); FWWB = fair-weather wave base. Data from Li et al. (2015).

Below the conglomerate bed, the uppermost strata of member 3 are composed mainly of floatstones or packstones, which contain nummulitids. This interval records the progressive transition to open-marine environments, with the uppermost strata deposited below fair-weather wave base (Fig. 3C).

The ≤4 m thick conglomerate bed, found marking the boundary between members 3 and 4 of the Zongpu Formation in the Gamba area, is markedly lenticular in shape, with a sharp erosional base and flat, normally-graded top (Fig. 2A, E). Clasts are mostly subrounded to rounded, though some angular clasts are present. They range in diameter from 0.5 to 15 cm, and consist mainly of coarse-grained, nummulitid-bearings wackestones and packstones derived from the coeval (or slightly older) Thanetian limestones of member 3 (Fig. 3B). The poor sorting, homogeneous character of the clasts, and presence of some angular fragments suggests a local source area, and possibly rapid transport and deposition. The occurrence of rounded clasts does imply some transport in a channel system, but not to the same degree that would be inferred from rounded silicate clasts, since limestone pebbles are rounded quite easily by mechanical abrasion (Kuenen, 1964; Mills, 1979). The lenticular bedding and erosive contact with underlying strata both indicate deposition by bedload traction in a high energy, channelized flow. The thicker, more laterally continuous conglomerate units are interpreted to have been deposited in an incised channel, within a braided channel system (Wang et al., 2010; Li et al., 2015).

Above the conglomerate bed, the base of member 4 consists mainly of restricted to lagoonal inner-ramp deposits, characterized by *Alveolina* and *Orbitolites*. These transition up-section into shallow-marine deposits, and finally open-marine floatstones with *Nummulites* and *Alveolina*, deposited below wave base in a middle ramp environment (Fig. 3A).

4.2. Biostratigraphy

The biostratigraphy of the Upper Cretaceous to lower Paleogene shallow-water succession of the Tibetan Himalaya is described in detail in BouDagher-Fadel et al. (2015), which correlated the planktonic foraminiferal zones of BouDagher-Fadel (2013) and the shallow benthic foraminiferal zones of the Paleogene into a comprehensive new Tibetan biozonation scheme (Fig. 4). Here we focus on: 1) the stratigraphic interval spanning the Paleocene-Eocene boundary, and 2) the biostratigraphic features of the Paleocene-Eocene disconformity.

In both studied sections, the boundary between SBZ3 and SBZ4 (or TP2 and TP3) is defined by the first appearance of *Aberisphaera gambanica*. Within SBZ4/TP3, *Lockhartia conditi*, *Lockhartia haimei*, *Lockhartia cushmani*, *Daviesina langhami* (Fig. 5A), *Orbitosiphon punjabensis* (Fig. 5B), *Ranikothalia sindensis* (Fig. 5C–a), *Orbitosiphon praepunjabensis* (Fig. 5C-b), *Miscellanea juliettae* (Fig. 5D), *Lockhartia roeae* (Fig. 5C-d) and *Miscellanea yvettae* (Fig. 5E) are common. The first appearance of *Alveolina pasticillata* and *Alveolina ellipsoidalis* (Fig. 5F-b) marks the base of TP5 (within the lower part of SBZ6), corresponding to the base of the Ypresian. This subzone is dominated by *Orbitolites complanatus* (Fig. 5F–a), *Glomalveolina subtilis*, *Alveolina pasticillata*, *Alveolina ellipsoidalis* (Fig. 5H), *Alveolina aramaea* and *Alveolina illerdensis*. The boundary between SBZ6 and SBZ7 is marked by the first appearance of *Alveolina moussoulensis*.

Carbonate clasts from the conglomerate bed in the Gamba area yielded SBZ 4 to SBZ 6 index fossils, including *Lockhartia haimei*, *Lockhartia conditi*, *Daviesina langhami*, *Miscellanea juliettae* and *M. yvettae* in SBZ4, *Alveolina vredenburgi* in SBZ5, and *Orbitolites complanatus* and *Alveolina ellipsoidalis* in SBZ 6 (Fig. 3, Fig. 5G).

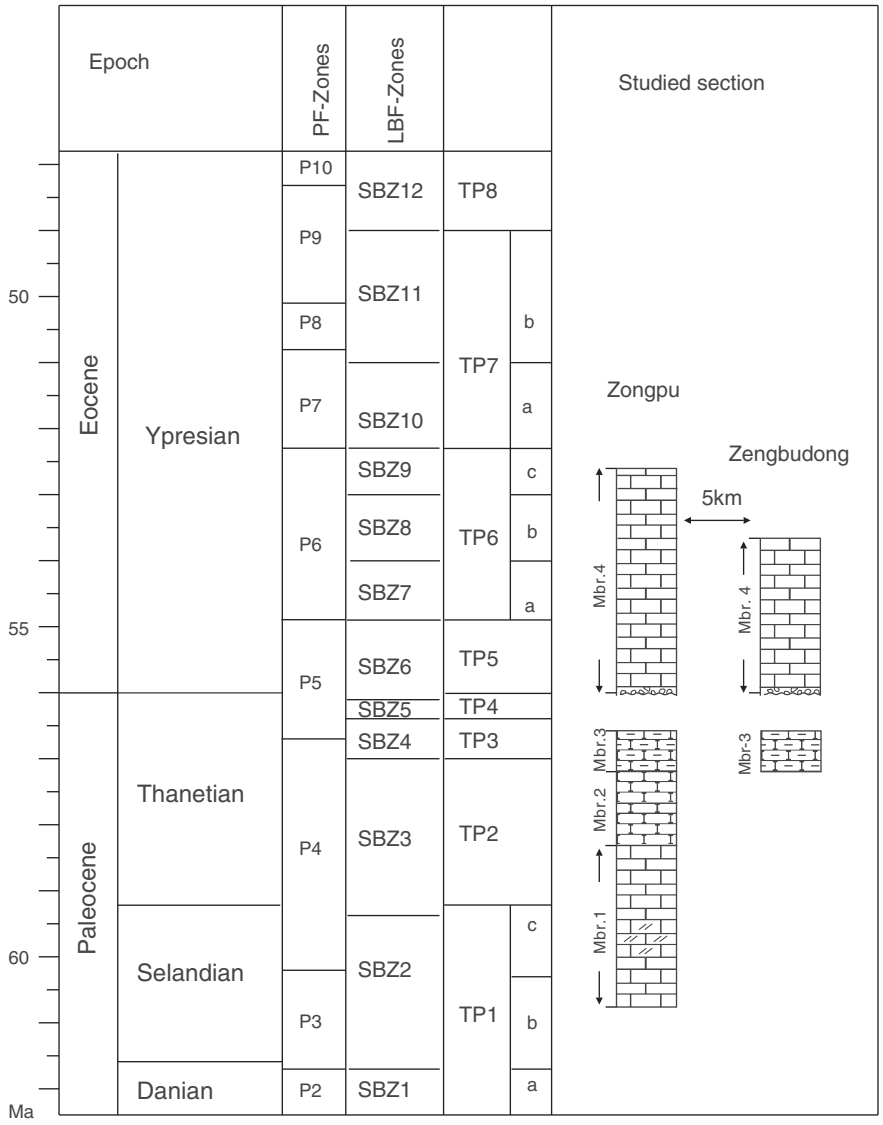

Fig. 4. Integrated chrono- and biostratigraphic framework for the Gamba sections of the southern Tethyan Himalaya. Planktonic foraminiferal biozones from BouDagher-Fadel (2013); larger benthic foraminiferal biozones from BouDagher-Fadel (2008, 2015). Timescale is based on Gradstein et al. (2012). Legend corresponds to that in Fig. 3.

4.3. Stable carbon isotope stratigraphy

Stable carbon isotope values are plotted stratigraphically in Fig. 6 for the Zongpu section and Fig. 7 for the Zengbudong section. The lower Thanetian is characterized by high variability in whole-rock carbonate isotope values, while the upper Thanetian and lower Eocene show $\delta^{13}C_{carb}$ values centered around +2‰ and +1‰, respectively, with an abrupt negative shift at the disconformable transition from open marine to restricted lagoonal deposits marked by the conglomerate bed (Figs. 6, 7). Above this negative excursion, a recovery trend is evident in both Zongpu and Zengbudong sections, beginning in the *Alveolina* packstone or floatstone at the base of member 4. The negative excursion in $\delta^{13}C_{carb}$ begins at 314.6 m in the Zongpu section ($\delta^{13}C_{carb} = -1.0‰$) and at 12.7 m in the Zengbudong section ($\delta^{13}C_{carb} = -2.4‰$), and persists over an interval of ~4 m in the Zongpu section, of ~5.4 m in the Zengbudong section. The magnitude of the CIE reaches 3.4‰ in the Zongpu section, and 4.9‰ in the Zengbudong section.

The organic carbon isotope values measured across the Paleocene-Eocene boundary in the Zengbudong section display a trend similar to the whole-rock carbonate record. In the upper part of member 3, $\delta^{13}C_{org}$ ranges from −22.1‰ to −21.6‰, with an average value of −21.8‰ (Fig. 7). An abrupt negative excursion, with a magnitude of 3‰, occurs at the base of member 4 (−24.6‰),. These ^{13}C–depleted values persist over a 5.4 m interval, then show a positive trend corresponding to that seen in carbonate isotopes, with values rising from −24.7‰ to −22.4‰.

The carbonate clasts in the conglomerate bed marking the Paleocene-Eocene boundary in the Zengbudong section are apparently altered, and display extreme $\delta^{13}C_{carb}$ values, ranging from −2.4‰ down to −6‰ (Fig. 8A). The organic carbon isotope values of the carbonate range vary from −23.0‰ to −25.1‰ (Fig. 8B).

5. The Paleocene–Eocene thermal event in the Himalaya

Previous studies of shallow-water successions in the Pyrenean Basin in Spain (Orue-Etxebarria et al., 2001; Pujalte et al., 2003, 2009, 2014, 2015, 2016), the Galala Mountains in Egypt (Scheibner et al., 2005; Scheibner and Speijer, 2009), the Adriatic carbonate platform in SW Slovenia (Zamagni et al., 2008, 2012), the Indus Basin in Pakistan (Afzal et al., 2011), the Zagros Basin in SW Iran (Bagherpour and Vaziri, 2012), and the Pacific region (Robinson, 2011), have extensively documented the correlation between the negative carbon isotope

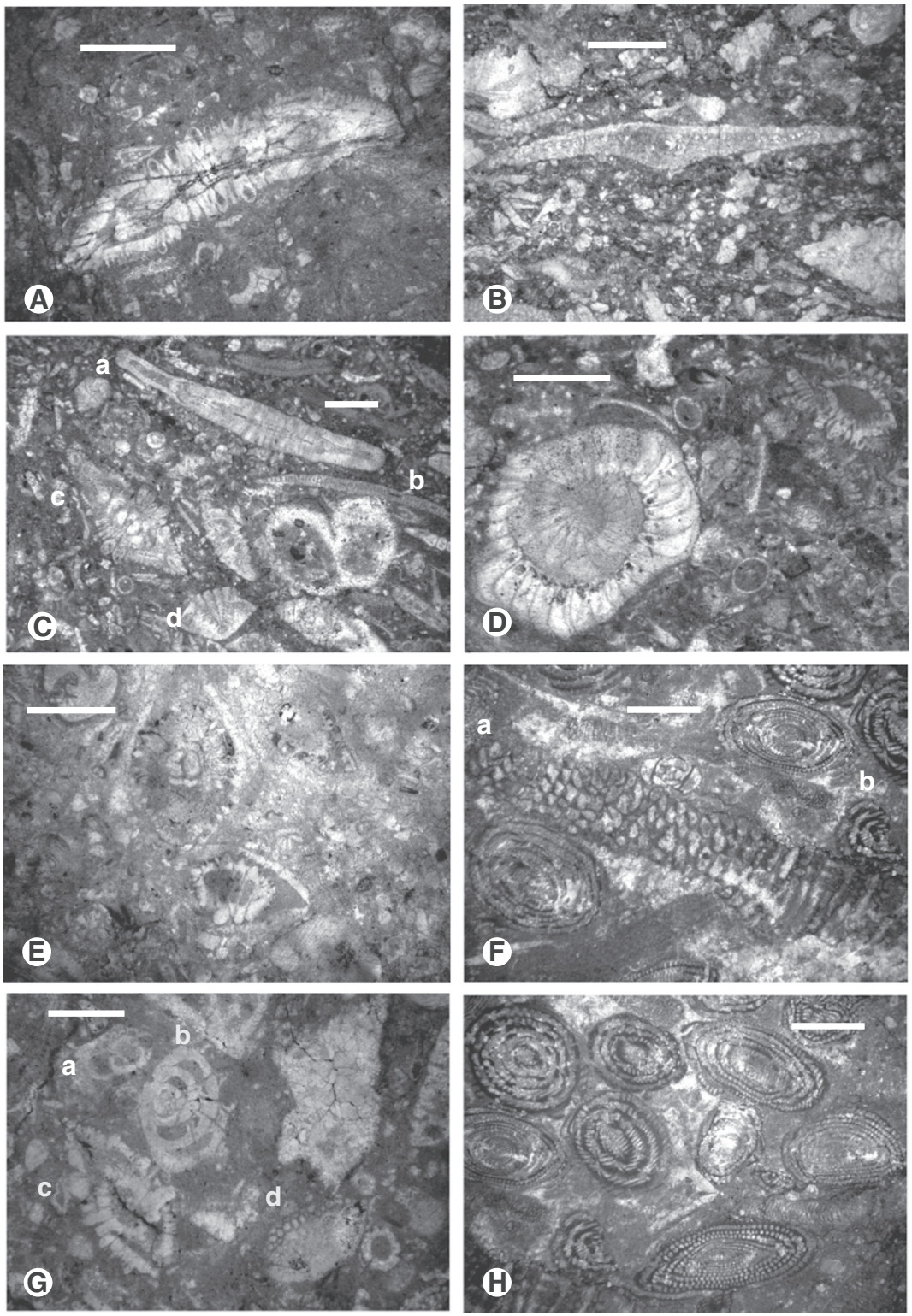

Fig. 5. Larger benthic foraminifera of SBZ4 through SBZ6 in the Zongpu and Zengbudong sections. A) *Daviesina langhami*, Thanetian, SBZ4, 12ZP133; B) *Orbitosiphon punjabensis*, Thanetian, SBZ4, 12ZP133; C) a. *Ranikothalia sindensis*, b. *Orbitosiphon praepunjabensis* Adams, c. *Miscellanea juliettae*, d. *Lockhartia roeae*, Thanetian, SBZ4, 12ZP182; D) *Miscellanea juliettae*, Thanetian, SBZ4, 12ZP182; E) *Miscellanea yvettae*, Thanetian, SBZ4, 12ZP229; F) a. *Orbitolites complanatus*, b. *Alveolina ellipsoidalis*, Ypresian, later part of SBZ6, 13ZB72; G) a. *Orbitosiphon punjabensis*, b. *Lockhartia conditi*, c. *Miscellanea miscella*, d. *Lockhartia diversa*, reworked late Thanetian SBZ4 assemblage mixed with early Ypresian assemblage, 12ZD69; H) *Alveolina ellipsoidalis* and *Alveolina pasticillata*, Ypresian, late SBZ6, 13ZB72.

excursion associated with the PETM and the evolution of larger benthic foraminifera. However, many of these studies were conducted in European and Mediterranean regions corresponding to the western Tethys; the applicability of Shallow Benthic Zones (SBZ) and regional biostratigraphic correlations to the shallow-water environments of the eastern Tethys remains uncertain (Wang et al., 2010), although Zhang et al. (2013) proposed a temporal correlation between the PETM and the evolution of larger benthic foraminifera in southern Tibet.

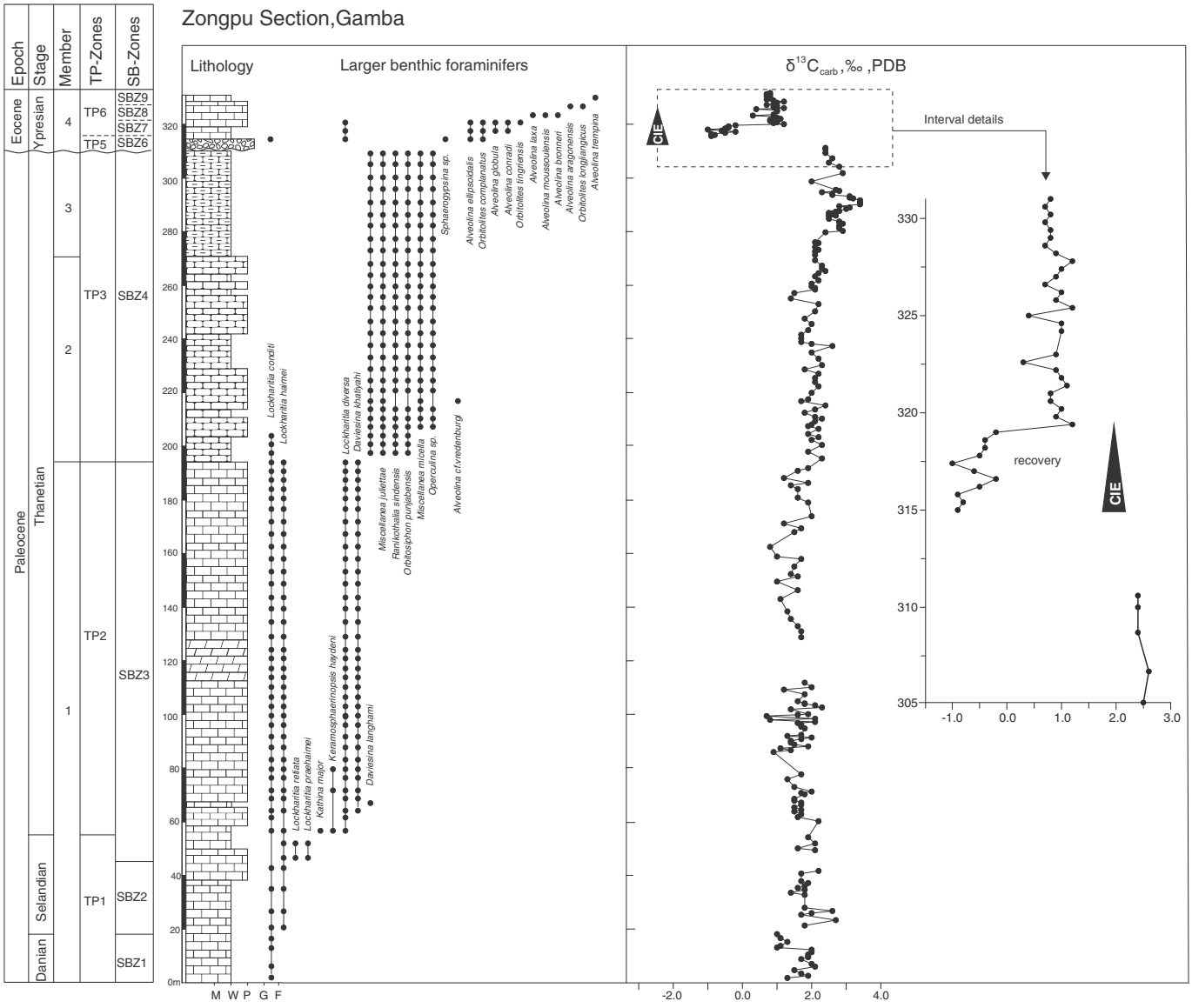

Fig. 6. Lithostratigraphy, biostratigraphic ranges of larger benthic foraminifera, and whole-rock carbonate $\delta^{13}C$ curve for the Zongpu section, Gamba area. SBZ = Shallow Benthic Zone, TP = Tibetan Foraminiferal Biozone, CIE = Carbon Isotopic Excursion; M = mudstone; W = wackestone; P = packstone; G = grainstone; F = floatstone. Legend corresponds to that in Fig. 3.

5.1. Diagenetic effects on carbon isotope curves

Dissolution and recrystallization processes during diagenesis of carbonate minerals can significantly alter their carbon isotope composition (Garzione et al., 2004). The carbon isotope ratio of authigenic carbonate may also change as a result of the transformation of aragonite and high-Mg calcite to low-Mg calcite during diagenesis, or from the presence of skeletal grains, which may exhibit nonequilibrium isotopic fractionation (Immenhauser et al., 2002; Swart and Eberli, 2005). Thin section analysis reveals that the carbonates of the Zongpu Formation are wackestones or packstones, with a homogeneous micritic matrix and skeletal grains. Microsparry calcite is rare, and sparry calcite is absent, indicating that the original sedimentary fabric has been largely preserved. The skeletal grains include both smaller and larger benthic foraminifera and echinoderms, and were originally composed of low-Mg to high-Mg calcite. Mineralogical stabilization of high-Mg calcite to low-Mg calcite can occur without any textural change in skeletal calcite, especially in porcellanaceous foraminifera like alveolinids and larger miliolids (Budd and Hiatt, 1993). In the absence of subaerial exposure, the transformation of high-Mg to low-Mg calcite occurs under the influence of marine pore waters, with only minor modification of the carbon isotope composition of skeletal grains. Overall, petrographic features suggest that carbonate strata in the studied sections have undergone minimal diagenetic alteration.

Measured $\delta^{13}C$ values range from −4.0‰ to 2.5‰, and $\delta^{18}O$ values range from −10‰ to −4‰. A crossplot of carbon and oxygen isotope values shows no significant correlation ($R^2 = 0.39$ for the Zongpu section; $R^2 = 0.02$ for the Zengbudong section; Fig. 8A). The crossplot also lacks the slope characteristic of "mixing lines" produced by the addition of variable quantities of cement to primary skeletal calcite (Marshall, 1992), suggesting that the isotopic values obtained from the studied sections likely record a primary palaeoceanographic signal.

5.2. Completeness of the PETM record in southern Tibet

The onset of the CIE and its shape are considered to be the most reliable correlation tools for the Paleocene-Eocene boundary interval

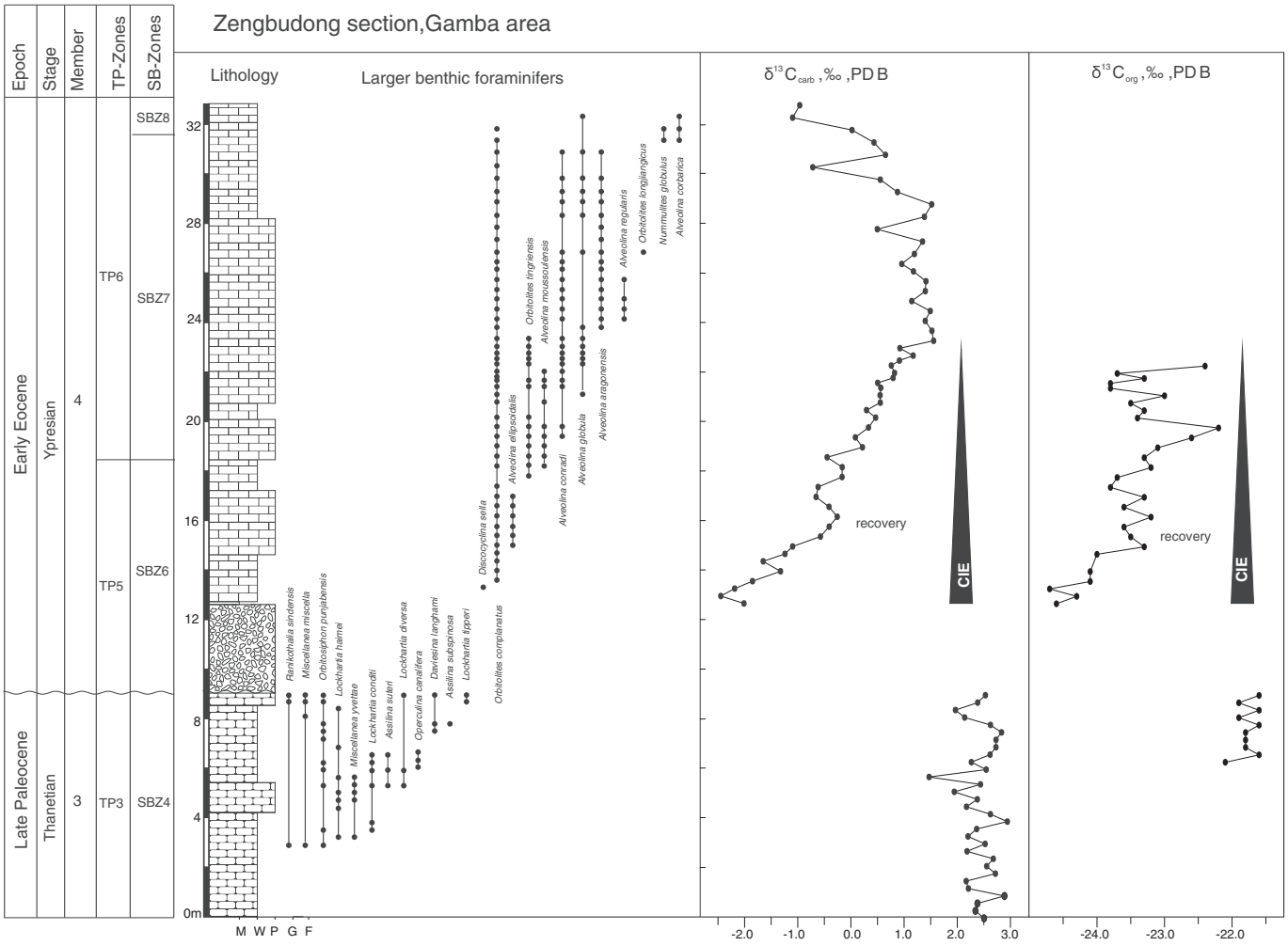

Fig. 7. Lithostratigraphy, biostratigraphic ranges of larger benthic foraminifera, and $\delta^{13}C$ curves for whole-rock carbonate and organic matter from the Zengbudong section, Gamba area.

(Röhl et al., 2007). The major environmental and biotic changes associated with the PETM provide additional criteria to both pinpoint the Paleocene-Eocene boundary and assess the stratigraphic completeness of the PETM event as recorded in south Tibet.

In both studied sections of the Zongpu Formation, sedimentological and biostratigraphic analyses indicate a major erosional unconformity between the top of member 3 (which dates to the latest Paleocene SBZ 4), and the base of member 4 (which dates to the early Ypresian

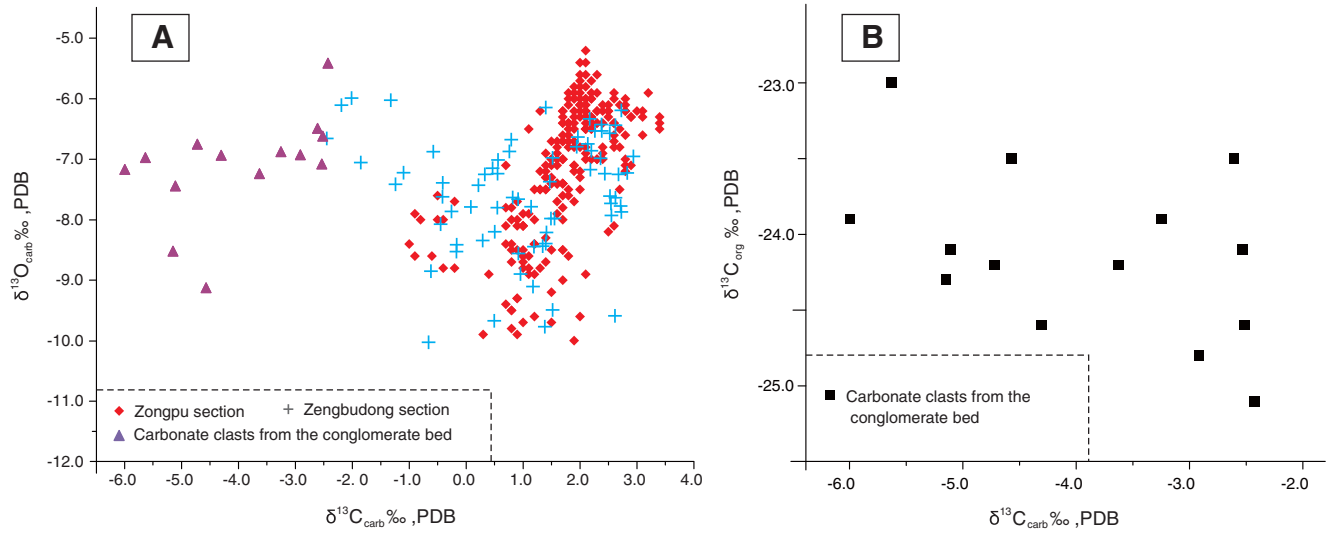

Fig. 8. Crossplots of: A) Whole-rock carbonate carbon versus oxygen isotopes ($\delta^{13}C$ vs. $\delta^{18}O$) from the Zongpu Formation, in the Zongpu and Zengbudong sections; B) Whole-rock carbonate carbon versus organic carbon isotopes ($\delta^{13}C_{carb}$ vs. $\delta^{13}C_{org}$) of carbonate clasts from the conglomerate bed in the Zengbudong section.

SBZ 6). This disconformity should thus represent at least 400 kyr, corresponding to the missing SBZ5 and the earliest part of SBZ6 (BouDagher-Fadel, 2008; Fig. 4). Analysis of carbonate clasts contained in the conglomerate bed helps to further constrain the time interval represented by the disconformity, and to assess the processes driving this erosion. Intraformational carbonate clasts include index fossils from SBZ4 through SBZ6 (Fig. 3). The sedimentary record of the Paleocene-Eocene boundary within SBZ6 (BouDagher-Fadel, 2008), including the onset of the PETM, was thus truncated by latest Paleocene erosion.

The discontinuity of the sedimentary record is highlighted by the abruptness of the isotopic excursion. In southern Tibet, the negative $\delta^{13}C_{carb}$ and $\delta^{13}C_{org}$ excursions are extremely sharp (from 2.5 to - 2.0‰ and from −21.6 to −24.6‰, respectively), consistent with the presence of a hiatus. The base of the Eocene in the Gamba area also shows a sudden change from open marine to restricted-lagoonal environments. Both $\delta^{13}C_{carb}$ and $\delta^{13}C_{org}$ values remain consistent or increase slightly immediately below the conglomerate bed, implying that the onset of the CIE is not recorded in these strata. The 4 to 7 m thick interval with consistently low $\delta^{13}C_{carb}$ and $\delta^{13}C_{org}$ values (i.e., the CIE) is followed by a gradual return to pre-excursion values (Figs. 6, 7, 9), suggesting that while the onset of the PETM is truncated by erosion, the stratigraphic record of the upper PETM interval is expanded and continuous.

5.3. Comparison between southern Tibet and other marine successions

Constraining the magnitude of the CIE is critical to evaluating its potential causes (Higgins and Schrag, 2006) and understanding the sensitivity of the climate system to the associated greenhouse gas forcing. Measurements vary widely, ranging from 2‰ to 4.5‰ in marine carbonates depending on the studied location and substrate (Giusberti et al., 2007; Sluijs and Dickens, 2012). The observed magnitude of the negative excursion in our whole-rock carbonate records (~3.4‰ in the Zongpu section and ~4.9‰ in the Zengbudong section) is slightly greater than the values reported from other shallow-marine continental margins (e.g., between 2.8‰ and 3.5‰ for the North American shelf; John et al., 2008), the Adriatic carbonate platform (~1‰ in the Kozina section and ~3‰ in the Čebulovica section; Zamagni et al., 2012), Pacific guyots (~3‰; Robinson, 2011), and deep-sea bulk carbonates (between 2.5‰ and 4.0‰).

The magnitude of the negative CIE in our shallow-marine carbonate record is quite large compared to open-marine records of the PETM, with an excursion in whole-rock carbonate samples of up to 4.9‰ in the Zengbudong section (Fig. 10). The low $\delta^{13}C$ values of these carbonates may be due to a combination of several effects, including restricted circulation and a smaller carbon reservoir size in the platform-top water mass, a local flux of carbon weathering from the land, and syndepositional diagenesis of carbonate mud in organic-rich sediments (Immenhauser et al., 2008).

In the Gamba area, the Zongpu Formation was deposited in a carbonate ramp setting characterized by good water circulation, suggesting that water mass restriction was not a major factor. Low pore water $\delta^{13}C$ values may have resulted from the oxidation of organic matter. Syndepositional dissolution of $CaCO_3$ caused by organic matter oxidation can alter the isotopic composition of carbonate, resulting in lower $\delta^{13}C$ values in diagenetic carbonates (Sanders, 2003; Patterson and Walter, 1994). The strongly negative excursions in whole-rock $\delta^{13}C_{carb}$ values observed in the Zongpu Formation may reflect syndepositional alteration of organic matter. Climatic conditions during the PETM, with intensified chemical weathering and seasonality driving more efficient physical weathering and erosion (Egger et al., 2005; Giusberti et al., 2007), promoted the accumulation of organic-rich black shales along the margin of the Neo-Tethys Ocean (Speijer and Wagner, 2002). Current-driven redistribution of organic matter along the carbonate ramp may have contributed to the differences in the magnitude of negative carbon isotope excursions observed between the Zongpu and Zengbudong sections, with the former characterized by less negative $\delta^{13}C_{carb}$ values.

6. Origin of the P-E boundary unconformity

The channelized intraformational conglomerate bed that marks the boundary between members 3 and 4 of the Zongpu Formation in the Gamba area has long been biostratigraphically correlated with a similar unit in the Zanskar Range of the northwestern Tethyan Himalaya. This conglomerate is interpreted to be the result of tectonic uplift, due to landward migration of a collision-related flexural wave (Garzanti et al., 1987). The same mechanism has been proposed to explain the conglomerate bed in the Gamba area (Zhang et al., 2012; Li et al., 2015), and a similar disconformity and conglomerate bed can be observed in the Tingri and Düela areas (unpublished field observations). The Paleocene-Eocene erosional unconformity is not limited to the Gamba area, but can be traced for 200 km across southern Tibet. Considering the similarity between stratigraphic records in the Gamba area and the Zanskar Range, we conclude that this Paleocene-Eocene disconformity is a widespread, roughly synchronous feature in the Tethyan Himalaya. The combination of biostratigraphy and detailed carbon isotope chronostratigraphy presented in this study allow us to establish that this erosional event occurred during the lower PETM interval (i.e., around 56 or 55.5 Ma; Hilgen et al., 2010; Westerhold et al., 2012).

The origin of the Paleocene-Eocene boundary unconformity in the Tethyan Himalaya is discussed below, in relation to: 1) tectonic uplift

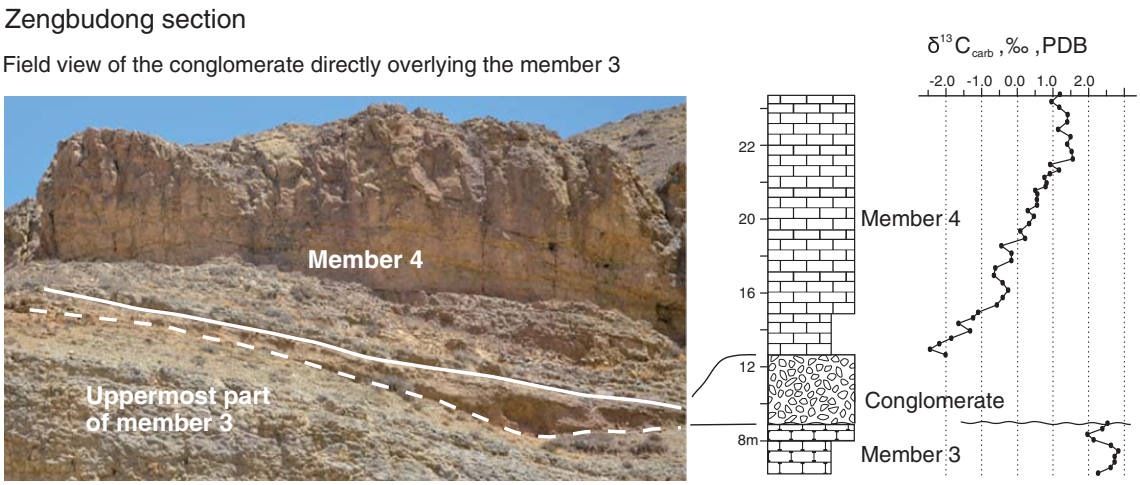

Fig. 9. Integrated field photography, lithological log, and stable isotope curve from the Zengbudong section, spanning the Paleocene/Eocene boundary in the Gamba area, southern Tibet.

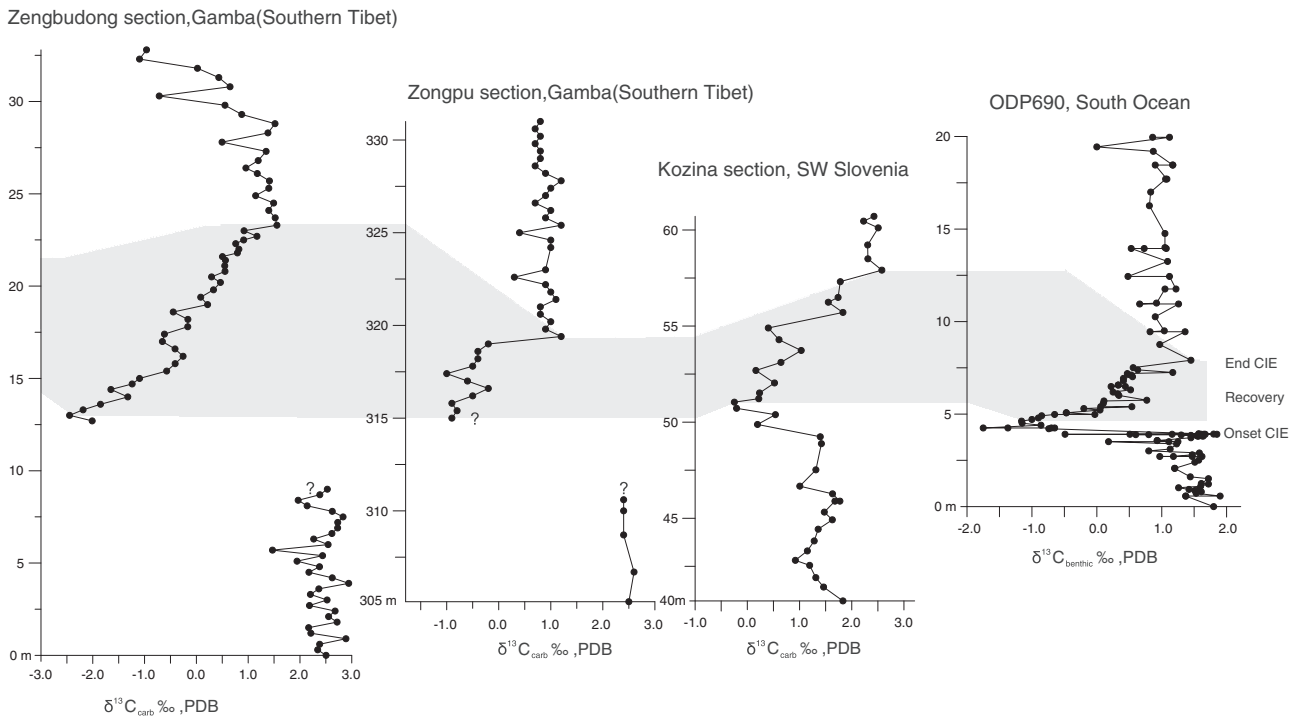

Fig. 10. Chemostratigraphic correlation of PETM records based on stable carbon isotopes, from the Gamba area of southern Tibet (this study), Kozina, SW Slovenia (Zamagni et al., 2012), and the Southern Ocean (ODP690; Kennett and Stott, 1991).

of the Zongpu carbonate platform, and 2) climate-driven incision and erosion prior to the PETM.

6.1. Tectonic uplift of the Zongpu platform

Based on evidence from the northwestern Himalaya, Garzanti et al. (1987) proposed that the Indian passive margin was tectonically uplifted by southward migration of an orogenic wave that initiated at the Trans-Himalayan Trench during the onset of the collision between India and Asia. In depositional settings from the outer Indian margin, exposed in the Zanskar Range, pelagic outer-shelf sediments yielding planktonic foraminifera of Thanetian age are unconformably overlain by peritidal dolostones and nummulitid-rich calcarenite shoals of early Ypresian age. Channelized quartz-rich sandstone beds are reported to occur during the same interval in the inner Zanskar margin (Nicora et al., 1987), whereas debris-flow conglomerates containing limestone pebbles of Cretaceous to latest Paleocene age occur in the most distal part of the Indian margin (Fuchs and Willems, 1990).

In the Gamba sections of southern Tibet, the unusually low carbon isotope values of conglomerate clasts ($\delta^{13}C$ as negative as −6‰ PDB; Fig. 8) suggests a period of weathering and freshwater influx associated with prolonged subaerial exposure (Immenhauser et al., 2002). This interpretation is strongly supported by three independent lines of evidence: 1) the presence of channelized intraformational conglomerates mantling a major stratigraphic disconformity; 2) a stratigraphic gap of ~400 kyr, corresponding to the missing SBZ5; and 3) a sharp break in the $\delta^{13}C_{carb}$ record, documented in all studied sections. Facies analysis, biostratigraphy, and carbon isotope measurements thus provide compelling evidence that, during a period of warm climate and sea level rise (Kominz et al., 2008; Sluijs et al., 2008), the Paleocene-Eocene disconformity was produced via tectonic uplift. Collision with Asia was already underway (DeCelles et al., 2014; Hu et al., 2015), and this marked uplift event recorded throughout the inner Tethyan Himalaya, from Zanskar to southern Tibet, may be the result of an orogenic wave propagating from the point of first continent-continent contact and moving progressively landward across the Indian margin.

Integrated biostratigraphic and zircon chronostratigraphic studies conducted on sedimentary successions from the most distal part of the Indian margin indicate that the onset of collision occurred in the Selandian (middle Paleocene) at 59 ± 1 Ma (DeCelles et al., 2014; Wu et al., 2014; Hu et al., 2015). If the unconformity was indeed caused by tectonic uplift related to a flexural wave, we can estimate the time required for the orogenic front to reach the inner Indian margin in Gamba, Tingri and Zanskar to be 3 ± 1 Myr. Assuming an original paleomargin width between 250 and 300 km (van Hinsbergen et al., 2012; Lippert et al., 2014), this corresponds to a migration velocity of 90 ± 20 km/Myr (mm/a). The convergence rate between India and Asia is estimated to have been ~150 mm/a based on paleomagnetic data (Copley et al., 2010; van Hinsbergen et al., 2011). A convergence/shortening ratio of 1.7 ± 1.0 is somewhat larger than what is typically observed in orogenic belts generated by continental collision, but with all of the uncertainties considered, it is still compatible with existing models (Doglioni et al., 2007).

6.2. Climate-driven incision and erosion prior to the PETM

It is widely understood that valleys in marine-basin margins are usually incised during periods of relative sea-level fall, and filled with sediments during the subsequent sea-level rise (Boyd et al., 2006; Strong and Paola, 2008; Pujalte et al., 2015). A sea-level lowstand preceding the PETM has been widely recognized; in the Pyrenees (Pujalte et al., 2014, 2015, 2016), the North Sea region (Dupuis et al., 2003), the Austrian Alps (northern margin of the Tethys, Egger et al., 2009; Egger, 2011), and the Nile Valley (southern margin of the Tethys, Aubry et al., 2009). This sea level fall was followed by an equally widespread sea-level rise.

In the Gamba area of the Tethyan Himalaya, the channelized intraformational conglomerate bed within the Paleocene-Eocene boundary interval of the Zongpu Formation also marks the boundary between the open-marine environments of member 3 and the restricted to lagoonal inner-ramp deposits of member 4. The roughly coeval disconformity in the Zanskar Range (Garzanti et al., 1987) clearly

records a pronounced fall in relative sea-level, and consequently the formation of an incised valley in previously deposited carbonate-ramp strata (Li et al., 2015). The subsequent rise in relative sea-level began ~40 kyr before the Paleocene–Eocene boundary, leading to the filling of incised valleys and deposition of the conglomerate bed. Relative sea-level continued to rise during and after the PETM, leading to the deposition of floatstones containing *Alveolina* and *Orbitolites* in member 4 of the Zongpu Formation. Deposition of the conglomerate bed, which sedimentological evidence suggests may have occurred in a fluvio-deltaic or shallow-marine environment, would have had to have been rapid in this scenario.

The tectonic and eustatic components of base-level change cannot be easily distinguished in the stratigraphic record, and we are unable to deconvolve their relative contributions to the formation of the Paleocene-Eocene disconformity. The unique features of the conglomerate bed, which has no equivalent in the underlying Paleocene succession, point to a single specific event driving subaerial exposure and erosion. Tectonic activity was certainly underway during these earliest stages of the India-Asia collision, and therefore tectonic reduction of accommodation space remains a viable explanation. This is especially true of the disconformity in the Zanskar region, which separates pelagic marly limestones below from peritidal carbonates above, suggesting a drastic relative sea-level fall of at least 100 m. Glacio-eustasy is a mechanism capable of driving large and rapid fluctuations in sea-level, but can be ruled out due to the extremely warm climatic conditions around the Paleocene-Eocene boundary. The aquifer-eustasy hypothesis (Wendler and Wendler, 2016) has yet to be proven as a workable alternative mechanism. However, we have no evidence to rule out a climatically-driven eustatic component, and further work is needed to better understand the possibly superimposed processes that drove deep incision and erosion along the inner margin of the Tethyan Himalaya prior to the PETM.

7. Conclusions

This study reports a detailed stratigraphic record of the Paleocene–Eocene Thermal Maximum from the Tethyan Himalaya. The succession is truncated by a major disconformity around the Paleocene-Eocene boundary, marked by a conglomerate bed now identified in both the Gamba and Tingri areas of southern Tibet. As a result of this unconformity, only the upper part of the PETM interval is preserved. By coupling sedimentological, biostratigraphic, and geochemical data, we were able to reconstruct in detail the sedimentary and tectonic evolution of the southern Indian margin during the earliest stages of the India-Asia collision. Our results allows us to conclude that:

1) The Paleocene-Eocene unconformity corresponds with the boundary between members 3 and 4 of the Zongpu Formation, documenting an abrupt environmental change from open-marine environments below to restricted or lagoonal inner-ramp environments above. The prominent negative excursion in $\delta^{13}C$ at the base of member 4 is seen in both whole-rock carbonate and organic carbon records, and can correlated using larger-benthic-foraminifera biostratigraphy with the carbon isotope excursion defining the PETM. The strong ^{13}C depletion seen in shallow-marine carbonates in southern Tibet may have resulted partly from syndepositional alteration of organic matter.
2) The marked negative shift in carbon isotope values across the Paleocene-Eocene boundary is associated with conglomerate beds in the Gamba area of southern Tibet, and a stratigraphic gap of as much as 400 kyr, providing compelling evidence of subaerial exposure. This major Paleocene-Eocene disconformity may be ascribed to tectonic uplift associated with the southward migration of an orogenic wave that originated 3 ± 1 Myr earlier, as India began to collide with Asia in the middle Paleocene. Eustatic sea-level fall may have caused the incision of valleys prior to the PETM, with subsequent filling of the valleys during the interval of conglomerate deposition, however the impact of eustasy on the stratigraphy of the Tethyan Himalaya requires further study.

Acknowledgments

We would like to express our gratitude to Wei An, Zhong Han, and Mingyuan Lai for their assistance in the field and the laboratory for Provenance Studies, and to Carlo Doglioni, Shijun Jiang, Yongxiang Li and Jiangang Wang for their advice in preparing this manuscript. This study was financially supported by the National Natural Science Fund for Distinguished Young Scholars (41525007) and the Chinese MOST 973 Project (2012CB822001). We would also like to thank our two reviewers and Editor Prof. Isabel Patricia Montanez for their constructive comments.

Appendix A. Supplementary data

Supplementary data to this article can be found online at http://dx.doi.org/10.1016/j.palaeo.2016.11.026.

References

Afzal, J., Williams, M., Leng, M.J., Aldridge, R.J., Stephenson, M.H., 2011. Evolution of Paleocene to Early Eocene larger benthic foraminifer assemblages of the Indus Basin, Pakistan. Lethaia 44, 299–320.
Aubry, M.P., Dupuis, C., Berggren, W.A., Ouda, K., Knox, K., Sabour, A.A., 2009. Sea-level changes bracket the PETM. In: Strong, P., Crouch, E., Hollis, C. (Eds.), Biotic Events of the Paleogene, CBEP 2009. Conference program and Abstracts, Wellington, New Zealand, p. 144.
Aubry, M.P., Ouda, K., Dupuis, C., Berggren, W.A., Couvering, J.A.V., 2007. The Global Standard Stratotype-section and Point (GSSP) for the base of the Eocene Series in the Dababiya section (Egypt). Episodes 30 (4), 271.
Bagherpour, B., Vaziri, M.R., 2012. Facies, paleoenvironment, carbonate platform and facies changes across Paleocene Eocene of the Taleh Zang Formation in the Zagros Basin, SW-Iran. Hist. Biol. 24, 121–142.
BouDagher-Fadel, M.K., 2008. Evolution and Geological Significance of Larger Benthic Foraminifera: Developments in Paleontology and Stratigraphy. Volume 21. Elsevier, Amsterdam (540 p).
BouDagher-Fadel, M.K., 2013. Biostratigraphic and Geological Significance of Planktonic Foraminifera. second ed. OVPR University College of London, London (307 p).
BouDagher-Fadel, M.K., Price, G.D., Hu, X., Li, J., 2015. Late Cretaceous to early Paleogene foraminiferal biozones in the Tibetan Himalayas, and a pan-Tethyan foraminiferal correlation scheme. Stratigraphy 12, 67–91.
Bowen, G.J., Bralower, T.J., Delaney, M.L., Dickens, G.R., Kelly, D.C., Koch, P.L., et al., 2006. Eocene hyperthermal event offers insight into greenhouse warming. EOS Trans. Am. Geophys. Union 87, 165–169.
Boyd, R., Dalrymple, R.W., Zaitlin, B.A., 2006. Estuarine and incised-valley facies models. In: Posamentier, H.W., Walker, R.G. (Eds.), Facies Models Revisited vol 84. SEPM Sp. Pub., pp. 171–235.
Budd, A.D., Hiatt, E.E., 1993. Mineralogical stabilization of high-magnesium calcite—geochemical evidence for intracrystal recrystallization within Holocene porcellaneous foraminifera. J. Sediment. Petrol. 63, 261–274.
Copley, A., Avouac, J.P., Royer, J.Y., 2010. India-Asia collision and the Cenozoic slowdown of the Indian plate: Implications for the forces driving plate motions. J. Geophys. Res. Solid Earth vol 115 (B3) (1978–2012).
DeCelles, P., Kapp, P., Gehrels, G., Ding, L., 2014. Paleocene-Eocene foreland basin evolution in the Himalaya of southern Tibet and Nepal: implications for the age of initial India-Asia collision. Tectonics 33 (5), 824–849.
Dickens, G.R., Castillo, M.M., Walker, G., 1997. A blast of gas in the latest Paleocene: Simulating first-order effects of massive dissociation of oceanic methane hydrate. Geology 25 (3), 259–262.
Doglioni, C., Carminati, E., Cuffaro, M., Scrocca, D., 2007. Subduction kinematics and dynamic constraints. Earth Sci. Rev. 83 (3), 125–175.
Dupuis, C., Aubry, M.P., Steurbaut, E., Berggren, W.A., Ouda, K., Magioncalda, R., Cramer, B.S., Kent, D.V., Speijer, R.P., Heilmann-Clausen, C., 2003. The Dababiya Quarry section: lithostratigraphy, clay mineralogy, geochemistry and paleontology. Micropaleontology 49, 41–59.
Egger, H., 2011. The early Paleogene history of the Eastern Alps. In: Egger, H. (Ed.), Climate and Biota of the Early Paleogene, Field-Trip Guidebook, Salzburg, Austria. Berichte der Geologischen Bundesanstalt. vol 86, pp. 9–16.
Egger, H., Heilmann-Clausen, C., Schmitz, B., 2009. From shelf to abyss: record of the Paleocene/Eocene boundary in the Eastern Alps (Austria). Geol. Acta 7, 215–227.
Egger, H., Homayoun, M., Huber, H., Rögl, F., Schmitz, B., 2005. Early Eocene climatic, volcanic, and biotic events in the northwestern Tethyan Untersberg section, Austria. Palaeogeogr. Palaeoclimatol. Palaeoecol. 217 (3–4), 243–264.

Fuchs, G., Willems, H., 1990. The final stages of sedimentation in the Tethyan Zone of Zanskar and their geodynamic significance (Ladakh-Himalaya). Jahrb. Geol. Bundesanst. 133, 259–273.
Garzanti, E., Hu, X., 2015. Latest Cretaceous Himalayan tectonics: obduction, collision or deccan-related uplift? Gondwana Res. 28 (1), 165–178.
Garzanti, E., Baud, A., Mascle, G., 1987. Sedimentary record of the northward flight of India and its collision with Eurasia (Ladakh Himalaya, India). Geodin. Acta 1, 297–312.
Garzione, C.N., Dettman, D.L., Horton, B.K., 2004. Carbonate oxygen isotope paleoaltimetry: evaluating the effect of diagenesis on paleoelevation estimates for the Tibetan plateau. Palaeogeogr. Palaeoclimatol. Palaeoecol. 212 (1), 119–140.
Giusberti, L., Rio, D., Agnini, C., Backman, J., Fornaciari, E., Tateo, F., Oddone, M., 2007. Mode and tempo of the Paleocene-Eocene thermal maximum in an expanded section from the Venetian pre-Alps. Geol. Soc. Am. Bull. 119 (3–4), 391–412.
Gradstein, F.M., Ogg, J.G., Schmitz, M., Ogg, G., 2012. The geologic time scale 2012. 2-volume set. elsevier.
Higgins, J.A., Schrag, D.P., 2006. Beyond methane: towards a theory for the Paleocene–Eocene thermal maximum. Earth Planet. Sci. Lett. 245 (3–4), 523–537.
Hilgen, F.J., Kuiper, K.F., Lourens, L.J., 2010. Evaluation of the astronomical time scale for the Paleocene and earliest Eocene. Earth Planet. Sci. Lett. 300 (1), 139–151.
Hottinger, L., 1960. Uber Eocane und Paleocane Alveolinen. Eclogae Geol. Helv. 53, 265–283.
Hu, X., Garzanti, E., Moore, T., Raffi, I., 2015. Direct stratigraphic dating of India-Asia collision onset at the Selandian (middle Paleocene, 59 ± 1 Ma). Geology 43 (10), 859–862.
Hu, X., Sinclair, H.D., Wang, J., Jiang, H., Wu, F., 2012. Late Cretaceous-Palaeogene stratigraphic and basin evolution in the Zhepure Mountain of southern Tibet: implications for the timing of India-Asia initial collision. Basin Res. 24 (5), 520–543.
Immenhauser, A., Holmden, C., Patterson, W.P., 2008. Interpreting the carbon isotope record of ancient shallow epeiric seas: lessons from the recent. Geol. Assoc. Can. Spec. Pap. 48, 137–174.
Immenhauser, A., Kenter, J.A., Ganssen, G., Bahamonde, J.R., Van Vliet, A., Saher, M.H., 2002. Origin and significance of isotope shifts in Pennsylvanian carbonates (Asturias, NW Spain). J. Sediment. Res. 72 (1), 82–94.
John, C.M., Bohaty, S.M., Zachos, J.C., Sluijs, A., Gibbs, S., Brinkhuis, H., Bralower, T.J., 2008. North American continental margin records of the Paleocene-Eocene thermal maximum: implications for global carbon and hydrological cycling. Paleoceanography 23 (2), 1–20.
Kennett, J.P., Stott, L.D., 1991. Abrupt deep sea warming palaeoceanographic changes and benthic extinctions at the Palaeocene. Nature 353 (6341), 225–229.
Kominz, M.A., Browning, J.V., Miller, K.G., Sugarman, P.J., Mizintseva, S., Scotese, C.R., 2008. Late Cretaceous to Miocene sea-level estimates from the New Jersey and Delaware coastal plain coreholes: an error analysis. Basin Res. 20 (2), 211–226.
Kuenen, P.H., 1964. Experimental abrasion: 6. Surf action. Sedimentology 3 (1), 29–43.
Lippert, P.C., van Hinsbergen, D.J.J., Dupont-Nivet, G., 2014. Early Cretaceous to presentlatitude of the central proto-Tibetan Plateau: a paleomagnetic synthesis with implicationsfor Cenozoic tectonics, paleogeography, and climate of Asia. Geol. Soc. Am. Spec. Pap. 507.
Li, J., Hu, X., Garzanti, E., An, W., Wang, J., 2015. Paleogene carbonate microfacies and sandstone provenance (Gamba area, South Tibet): stratigraphic response to initial India–Asia continental collision. J. Asian Earth Sci. 104, 39–54.
Marshall, J.D., 1992. Climatic and oceanographic isotopic signals from the carbonate rock record and their preservation. Geol. Mag. 129 (2), 143–160.
McInerney, F.A., Wing, S.L., 2011. The Paleocene-Eocene thermal maximum: a perturbation of carbon cycle, climate, and biosphere with implications for the future. Annu. Rev. Earth Planet. Sci. 39, 489–516.
Mills, H.H., 1979. Downstream rounding of pebbles: a quantitative review. J. Sediment. Res. 49 (1), 295–302.
Murphy, B.H., Farley, K.A., Zachos, J.C., 2010. An extraterrestrial 3He-based timescale for the Paleocene–Eocene thermal maximum (PETM) from Walvis Ridge, IODP Site 1266. Geochim. Cosmochim. Acta 74 (17), 5098–5108.
Nicora, A., Garzanti, E., Fois, E., 1987. Evolution of the Tethys Himalaya continental shelf during Maastrichtian to Paleocene (Zanskar, India). Riv. Ital. Paleontol. Stratigr. 92, 439–496.
Orue-Etxebarria, X., Pujalte, V., Bernaola, G., Apellaniz, E., Baceta, J.I., Payros, A., NunÃez-Betelu, K., Serra-Kiel, J., Tosquella, J., 2001. Did the Late Paleocene thermal maximum affect the evolution of larger foraminifers? Evidence from calcareous plankton of the Campo Section (Pyrenees, Spain). Mar. Micropaleontol. 2001 (41), 45–71.
Patterson, W.P., Walter, L.M., 1994. Depletion of 13C in seawater CO2 on modern carbonate platforms: Significance for the carbon isotopie record of carbonates. Geology 22, 885–888.
Pujalte, V., Baceta, J.I., Schmitz, B., 2015. A massive input of coarse-grained siliciclastics in the Pyrenean Basin during the PETM: the missing ingredient in a coeval abrupt change in hydrological regime. Clim. Past 11 (12), 1653–1672.
Pujalte, V., Orue-Etxebarria, X., Schmitz, B., Tosquella, J., Baceta, J.I., Payros, A., Bernaola, G., Caballero, F., Apellaniz, E., 2003. Basal Ilerdian (earliest Eocene) turnover of larger foraminifera: Age constraints based on calcareous plankton and $\delta^{13}C$ isotopic profiles from new southern Pyrenean sections (Spain). Geol. Soc. Am. Spec. Pap. 369.
Pujalte, V., Robador, A., Payros, A., Samsó, J.M., 2016. A siliciclastic braid delta within a lower Paleogene carbonate platform (Ordesa-Monte Perdido National Park, southern Pyrenees, Spain): record of the Paleocene–Eocene thermal maximum perturbation. Palaeogeogr. Palaeoclimatol. Palaeoecol. 459, 453–470.
Pujalte, V., Schmitz, B., Baceta, J.I., 2014. . Sea-level changes across the Paleocene–Eocene interval in the Spanish Pyrenees, and their possible relationship with North Atlantic magmatism. Palaeogeogr. Palaeoclimatol. Palaeoecol. 393, 45–60.
Pujalte, V., Schmitz, B., Baceta, J.I., Orue-Etxebarria, X., Bernaola, G., Turell, J.D., Payros, A., Apellaniz, E., Caballero, F., 2009. Correlation of the Thanetian-Ilerdian turnover of larger foraminifera and the Paleocene-ocene thermal maximum:confirming evidence from the Campo area (Pyrenees, Spain). Geol. Acta 7 (1–2), 161–175.
Robinson, S.A., 2011. Shallow-water carbonate record of the Paleocene-Eocene Thermal Maximum from a Pacific Ocean guyot. Geology 39, 51–54.
Röhl, U., Westerhold, T., Bralower, T.J., Zachos, J.C., 2007. On the duration of the Paleocene-Eocene thermal maximum (PETM). Geochem. Geophys. Geosyst 8 (12), 1–13.
Sanders, D., 2003. Syndepositional dissolution of calcium carbonate in neritic carbonate environments: geological recognition, processes, potential significance. J. Afr. Earth Sci. 36 (3), 99–134.
Scheibner, C., Speijer, R.P., 2009. Recalibration of the Tethyan shallow-benthic zonation across the Paleocene-Eocene boundary: the Egyptian record. Geol. Acta 7 (1–2), 195–214.
Scheibner, C., Speijer, R.P., Marzouk, A.M., 2005. Turnover of larger foraminifera during the Paleocene-Eocene Thermal Maximum and paleoclimatic control on the evolution of platform ecosystems. Geology 33, 493–496.
Sciunnach, D., Garzanti, E., 2012. Subsidence history of the Tethys Himalaya. Earth-Sci. Rev. 111, 179–198.
Serra-Kiel, J., Hottinger, L., Caus, E., Drobne, K., Ferrandez, C., Jauhri, A.K., Less, G., Pavlovec, R., Pignatti, J., Samso, M.J., Schaub, H., Sirel, E., Strougo, A., Tambaregu, Y., Tosquella, J., Zakrevskaya, E., 1998. Larger foraminifera biostratigraphy of the Tethyan Paleoce`ne and Eocene. Bull. Soc. Geol. Fr. 169 (2), 281–299.
Sluijs, A., Dickens, G.R., 2012. Assessing offsets between the delta C-13 of sedimentary components and the global exogenic carbon pool across early Paleogene carbon cycle perturbations. Glob. Biogeochem. Cycles 26.
Sluijs, A., Bowen, G.J., Brinkhuis, H., Lourens, L.J., Thomas, E., 2007. The Palaeocene–Eocene thermal maximum super greenhouse: biotic and geochemical signatures, age models and mechanisms of global change. In: Williams, M., et al. (Eds.), Deep Time Perspectives on Climate Change: Marrying the Signal from Computer Models and Biological Proxies. Geol. Soc, London, pp. 323–347.
Sluijs, A., Brinkhuis, H., Crouch, E.M., John, C.M., Handley, L., Munsterman, D., Pancost, R.D., 2008. Eustatic variations during the Paleocene–Eocene greenhouse world. Paleoceanography 23 (4), PA4216. http://dx.doi.org/10.1029/2008PA001615.
Sluijs, A., Schouten, S., Pagani, M., Woltering, M., Brinkhuis, H., Damsté, J.S.S., Dickens, G.R., Huber, M., Reichart, G.J., Stein, R., Matthiessen, J., Lourens, L.J., Pedentchouk, N., Backman, J., Moran, K., the Expedition, 2006. Subtropical Arctic Ocean temperatures during the Palaeocene/Eocene thermal maximum. Nature 441 (7093), 610–613.
Speijer, R.P., Wagner, T., 2002. Sea-Level Changes and Black Shales Associated with the Late Paleocene Thermal Maximum: Organic-Geochemical and Micropaleontologic Evidence from the Southern Tethyan Margin (Egypt-Israel). Geol. Soc. Am. Spec. Pap.
Speijer, R.P., Scheibner, C., Stassen, P., Abdel-Mohsen, Morsi, 2012. Response of marine ecosystems to deep-time global warming: a synthesis of biotic patterns across the Paleocene-Eocene thermal maximum (PETM). Aust. J. Earth Sci. 105, 6–16.
Strong, N., Paola, C., 2008. Valleys that never were: time surfaces versus stratigraphic surfaces. J. Sediment. Res. 78, 579–593.
Swart, P.K., Eberli, G., 2005. The nature of the $\delta^{13}C$ of periplatform sediments: implications for stratigraphy and the global carbon cycle. Sediment. Geol. 175 (1–4), 115–129.
van Hinsbergen, D.J., Steinberger, B., Doubrovine, P.V., Gassmöller, R., 2011. Acceleration and deceleration of India-Asia convergence since the cretaceous: roles of mantle plumes and continental collision. J. Geophys. Res. Solid Earth 116 (B6).
Van Hinsbergen, D.J., Lippert, P.C., Dupont-Nivet, G., McQuarrie, N., Doubrovine, P.V., Spakman, W., Torsvik, T.H., 2012. Greater India Basin hypothesis and a two-stage Cenozoic collision between India and Asia. Proc. Natl. Acad. Sci. 109 (20), 7659–7664.
Wan, X.Q., Jansa, L.F., Sarti, M., 2002. Cretaceous-Paleogene boundary strata in southern Tibet and their implication for the India-Eurasia collision. Lethaia 35 (2), 131–146.
Wang, X., Wan, X.Q., Li, G.B., 2010. Turnover of larger benthic foraminifera during the Paleocene-Eocene stratigraphic boundary in Gamba, Tibet. Acta Micropalaeontologica Sin. 27 (2), 109–117.
Wendler, J.E., Wendler, I., 2016. What drove sea-level fluctuations during the mid-Cretaceous greenhouse climate? Palaeogeogr. Palaeoclimatol. Palaeoecol. 441, 412–419.
Westerhold, T., Röhl, U., Laskar, J., 2012. Time scale controversy: Accurate orbital calibration of the early Paleogene. Geochem. Geophys. Geosyst. 13 (6).
Willems, H., Zhang, B., 1993. Cretaceous and Lower Tertiary sediments of the Tibetan Tethys Himalaya in the area of Gamba (South Tibet, PR Chian). Berichte, Fachbereich Geowis senschaften, Universitat Bremen. 38, pp. 3–27.
Willems, H., Zhou, Z., Zhang, B., Gräfe, K.U., 1996. Stratigraphy of the Upper Cretaceous and Lower Tertiary strata in the Tethyan Himalayas of Tibet (Tingri area, China). Geol. Rundsch. 85, 723–754.
Wu, F.Y., Ji, W.Q., Wang, J.G., Liu, C.Z., Chung, S.L., Clift, P.D., 2014. Zircon U-Pb and Hf isotopic constraints on the onset time of India-Asia collision. Am. J. Sci. 314 (2), 548–579.
Yi, Z., Huang, B., Chen, J., Chen, L., Wang, H., 2011. Paleomagnetism of early Paleogene marine sediments in southern Tibet, China: Implications to onset of the India–Asia collision and size of Greater India. Earth Planet. Sci. Lett.
Zachos, J., Pagani, M., Sloan, L., Thomas, E., Billups, K., 2001. Trends, rhythms, and aberrations in global climate 65 Ma to present. Science 292 (5517), 686–693.

Zamagni, J., Mutti, M., Košir, A., 2008. Evolution of shallow benthic communities during the Late Paleocene–earliest Eocene transition in the Northern Tethys (SW Slovenia). Facies 54 (1), 25–43.

Zamagni, J., Mutti, M., Košir, A., 2012. The evolution of mid Paleocene-early Eocene coral communities: how to survive during rapid global warming. Palaeogeogr. Palaeoclimatol. Palaeoecol. 317-318, 48–65.

Zhang, Q., Willems, H., Ding, L., 2013. Evolution of the Paleocene-Early Eocene larger benthic foraminifera in the Tethyan Himalaya of Tibet, China. Int. J. Earth Sci. 102, 1427–1445.

Zhang, Q., Willems, H., Ding, L., Gräfe, K.U., Appel, E., 2012. Initial India-Asia continental collision and foreland basin evolution in the Tethyan Himalaya of Tibet: evidence from stratigraphy and paleontology. J. Geol. 120 (2), 175–189.